BIOCHEMISTRY
including biophysical chemistry & molecular biology
Article

Biochemistry **2010,** *49,* 6329–6340 6329
DOI: 10.1021/bi100339x

Characterization of Membrane Protein Non-native States. 2. The SDS-Unfolded States of Rhodopsin[†]

Arpana Dutta,[‡] Tai-Yang Kim,[§] Martina Moeller,[§] Jenny Wu,[‡,§] Ulrike Alexiev,*[,§] and Judith Klein-Seetharaman*[,‡]

[‡]*Department of Structural Biology, University of Pittsburgh School of Medicine, Pittsburgh, Pennsylvania 15260, and* [§]*Institut für Experimentalphysik, Freie Universität Berlin, Arnimallee 14, D-14195 Berlin, Germany*

Received March 5, 2010; Revised Manuscript Received June 22, 2010

ABSTRACT: Little is known about the molecular nature of residual structure in unfolded states of membrane proteins. A screen of chemical denaturants to maximally unfold the mammalian membrane protein and prototypic G protein coupled receptor rhodopsin, without interference from aggregation, described in an accompanying paper (DOI 10.1021/bi100338e), identified sodium dodecyl sulfate (SDS), alone or in combination with other chemicals, as the most suitable denaturant. Here, we initiate the biophysical characterization of SDS-denatured states of rhodopsin. Using absorption, steady-state and time-resolved fluorescence spectroscopy, dynamic light scattering, and cysteine accessibility studies, tertiary structure of denatured states was characterized. In agreement with the pattern of secondary structure changes detected by circular dichroism described in the accompanying paper (DOI 10.1021/bi100338e), tertiary structure changes are distinct over four SDS concentration ranges based on the expected predominant micellar structures. Dodecyl maltoside (DM)/SDS mixed micelle spheres (0.05−0.3% SDS) turn into SDS spheres (0.3−3% SDS) that gradually (3−15% SDS) become cylindrical (above 15% SDS). Denatured states in SDS spheres and cylinders show a relatively greater burial of cysteine and tryptophan residues and are more compact as compared to the states observed in mixed micellar structures. Protein structural changes at the membrane/water interface region are most prominent at very low SDS concentrations but reach transient stability in the compact conformations in SDS spheres. This is the first experimental evidence for the formation of a compact unfolding intermediate state with flexible surface elements in a membrane protein.

Membrane proteins are encoded by around 30% of the human genome. They function as important communication channels of the cell and its environment that aid in regulating the overall homeostasis of organisms. Understanding the pathway by which these proteins adopt a three-dimensional structure can provide us with key insights into the function of these proteins. The field of membrane protein folding is still at a nascent stage. Folding studies on bacteriorhodopsin, a bacterial membrane protein, have led to the formulation of the "two-stage hypothesis" (*1*). According to the two-stage model, helices are formed independently in the first stage. The second stage involves formation of tertiary contacts to generate the three-dimensional structure of a protein. However, *in vitro* and *in vivo* folding experiments and computational studies with the mammalian membrane protein rhodopsin have suggested that interactions between extracellular (EC)[1] and transmembrane (TM) domains are important in the early stages of folding (*2*−*5*). This forms the basis of a newer model of helical membrane protein folding, the "long-range interaction model" that emphasizes formation of a folding core-like structure in the initial stages of folding of rhodopsin (*2*). A systematic experimental characterization of secondary and tertiary structure changes during denaturation of rhodopsin leading to a largely unfolded state is required as a first step toward testing different models of membrane protein folding. Toward this goal, in an accompanying paper (DOI 10.1021/bi100338e), we have described the screening of different denaturing conditions for maximum unfolding without formation of aggregates. SDS was selected as a suitable detergent to further characterize unfolded states of rhodopsin. Its amphipathic character allows unfolding of both TM and water-exposed loop regions. It is also considered a suitable denaturant for membrane proteins due to its ability to unfold such proteins in their hydrophobic environment, thereby mimicking the conditions expected *in vivo*. The tertiary structure changes of SDS-induced unfolding were interpreted in light of changes in SDS micellar structure with increasing concentrations of SDS. SDS-induced tertiary structure changes, time-resolved and steady-state, were followed using (1) the absorption of the chromophore retinal as an intrinsic protein core probe, (2) the accessibility of surface-exposed and buried cysteines, (3) the emission changes of initially buried tryptophans, (4) change in the overall protein size, and (5) the dynamic changes of an amphiphatic lipid-anchored short helix that lies parallel to the membrane on the cytoplasmic side as a membrane/water interface probe. These studies constitute the first characterization of a stable unfolding intermediate of the membrane protein rhodopsin.

[†]This work was in part supported by National Science Foundation CAREER Grant CC044917, National Institutes of Health Grant NLM108730, and the Pennsylvania Department of Health to J.K.-S. and by the Deutsche Forschungsgesellschaft, Sfb 449, to U.A.

*To whom correspondence should be addressed. J.K.S.: tel, 412-383-7325; fax, 412-648-8998; e-mail, jks33@pitt.edu. U.A.: tel, 49-30-83855157; fax, 49-30-56510; e-mail, ulrike.alexiev@physik.fu-berlin.de.

[1]Abbreviations: SDS, sodium dodecyl sulfate; DM, dodecyl maltoside; 4-PDS, 4,4′-dipyridyl disulfide (alternative name: 4,4′-dithiodipyridine); IAF, 5-(iodoacetamido)fluorescein; CD, circular dichroism; MRE, mean residue ellipticity; EC, extracellular; TM, transmembrane.

Published on Web 06/24/2010

MATERIALS AND METHODS

Materials. SDS (electrophoresis grade) was purchased from Bio-Rad (Hercules, CA), dodecyl maltoside (DM) from Anatrace (Maumee, OH) and 4,4′-dithiodipyridine (4-PDS) from Sigma-Aldrich (St. Louis, MO). Silica beads from Polysciences Inc. (Warrington, PA) were a kind gift from Dr. Guillermo Calero at the University of Pittsburgh. Wild-type rhodopsin was isolated from bovine retinae and purified by immunoaffinity chromatography in 2 mM sodium phosphate buffer, pH 6, in the presence of 0.05% DM as described previously (*6*). The C140S/C316S mutant was constructed by cassette mutagenesis and expressed in COS-1 cells by transient transfection, followed by immunoaffinity chromatography as for the wild type (*6*). Fluorescence labeling of rhodopsin in position 316 with 5-(iodoacetamido)fluorescein (IAF; Molecular Probes) in DM micelles was carried out as described previously (*7*) following earlier protocols (*8*).

Methods. *Absorbance Spectroscopy*. UV−visible absorption spectra were recorded with a Perkin-Elmer λ 25 spectrophotometer (PerkinElmer, Waltham, MA). Measurements were taken at 25 °C using a 10 mm path length cell containing 1.5 μM purified rhodopsin in 2 mM sodium phosphate buffer, pH 6, and 0.05% DM in the absence and presence of SDS. All spectra were recorded with a bandwidth of 1 nm, response time of 1 s, and scan speed of 960 nm/min. The molar extinction coefficient used for rhodopsin at 500 nm is 40600 M^{-1} cm^{-1} (*9*). The time course of the appearance of a peak at 440 nm upon addition of 0.05% SDS was measured by repeated cycles.

Stopped-Flow Absorbance Spectroscopy. For faster kinetics, the appearance of the 440 nm peak on addition of SDS was recorded for samples containing 1.5 μM rhodopsin as a function of time using a Biologic (Grenoble, France) MOS-450 spectrometer equipped with a SFM-20 stopped-flow system. PMS-450 was used as the photomultiplier detector. Measurements were carried out at 25 °C. A total of 8000 data points were recorded for each SDS titration. The time trace obtained at each SDS concentration was fitted by a global fit of three spectra with a monoexponential function. In each case the error of the time constants was less than 4%. For reproducibility, a second set of measurements were performed at 1% SDS in a stopped-flow unit (SF61; HI-TECH Scientific) combined with a home-built transient absorption spectroscopy apparatus with microsecond time resolution.

Cysteine Reactivity. 4,4′-Dithiodipyridine (4-PDS) reacts with the free sulfhydryl groups in cysteines to produce stoichiometric amounts of 4-thiopyridone that absorbs at 323 nm (*10*). The number of cysteines reacting with 4-PDS per molecule of rhodopsin is estimated by taking the ratio of the absorbance at 323 nm and that at 500 nm and multiplying it with the ratio of the molar extinction coefficient of rhodopsin (40600 M^{-1} cm^{-1}) and that of 4-thiopyridone (19000 M^{-1} cm^{-1}). Rhodopsin (1.5 μM) in 2 mM sodium phosphate buffer, pH 6, and 0.05% DM was reacted with 37.5 μM 4-PDS in the sample cuvette at 25 °C. The same amount of 4-PDS was added to the reference cuvette. The reaction was followed spectrophotometrically by recording the changes in absorbance spectra over time. At the end of the experiment, when the 323 nm peak reached saturation, all spectra were subtracted from the original rhodopsin spectrum in the absence of 4-PDS. The 4-PDS reaction was carried out in the presence of different concentrations of SDS as indicated in the text and figure legends.

Steady-State Tryptophan Fluorescence Spectroscopy. Fluorescence measurements were carried out using a Varian Cary Eclipse fluorescence spectrophotometer (Varian Inc., Palo Alto, CA). Emission scans of 1.5 μM rhodopsin in 2 mM sodium phosphate buffer, pH 6, and 0.05% DM titrated with SDS in the presence and absence of 10 mM hydroxylamine were recorded in the wavelength range 310−500 nm with an excitation wavelength of 295 nm. Excitation and emission slit widths were kept at 5 and 10 nm (bandpass), respectively. Medium photomultiplier voltage was applied, and measurements were taken at a scan rate of 600 nm/min. For time course measurements, fluorescence emission at 330 nm was recorded every 30 min. All experiments were carried out at 25 °C.

Stopped-Flow Tryptophan Fluorescence Measurements. Rapid kinetics of increase in fluorescence on adding SDS to rhodopsin were measured on an Applied Photophysics SX18 spectrometer (Surrey, U.K.). All measurements were carried out at 25 °C. A total of 1000 data points were recorded for each SDS titration. An excitation wavelength of 295 nm and an emission cutoff filter of 320 nm were used. Both the emission and excitation slits were kept at 0.5 mm. All measurements were repeated three times. All curves were fitted with a sum of exponentials:

$$I(t) = \sum_{i=1} \alpha_i e^{-t/\tau_i} + c \quad (1)$$

where α_i are the amplitudes, τ_i are the time constant of each ith decay component, and c is the offset.

Dynamic Light Scattering. Dynamic light scattering measurements were performed using a DynaPro-99-E-50 instrument (Protein Solutions Inc., Charlottesville, VA). The buffer, 2 mM sodium phosphate, pH 6, was filtered through 0.22 μm syringe filters. Filtration of DM and SDS detergent solutions in the presence and absence of rhodopsin was avoided as it resulted in peaks of large hydrodynamic radius due to nonspecific reaction of the filter with the detergents. Viscosity coefficients of SDS solutions were obtained by measuring the diffusion coefficient of silica beads of 50 nm radius in water and in different SDS concentrations. Diffusion coefficients were obtained from the intensity autocorrelation function provided by the Dynamics V6 software supplied by the instrument manufacturer (Protein Solutions Inc., Charlottesville, VA). Viscosity coefficients were then calculated using the Stokes−Einstein equation. Hydrodynamic radii of 1.5 μM rhodopsin at varying concentrations of SDS were obtained by applying the Stokes−Einstein equation using Dynamics V6 software. All measurements were recorded at 25 °C.

Time-Resolved Fluorescence Depolarization. Fluorescence anisotropy decays were measured by employing a tunable Ti:sapphire laser/microchannel plate based single-photon counting apparatus with picosecond time resolution equipped with a TCSPC module (SPC-830; B&H GmbH) (*11*). The instrument response function of the system was ~35 ps (fwhm) at a channel width of 20 ps.

The fluorescence decay profiles ($I_{\parallel}(t)$ and $I_{\perp}(t)$) and the time-resolved anisotropy $r(t)$ as given by the equation

$$r(t) = \frac{I_{\parallel}(t) - I_{\perp}(t)}{I_{\parallel}(t) + 2I_{\perp}(t)} \quad (2)$$

were analyzed using the software package Global Unlimited V2.2. The time course of the fluorescence was fitted with a sum of exponentials:

$$I(t) = \sum_{i=1} \alpha_i e^{-t/\tau_i} \quad (3)$$

with α_i the amplitudes and τ_i the lifetimes of the ith decay component.

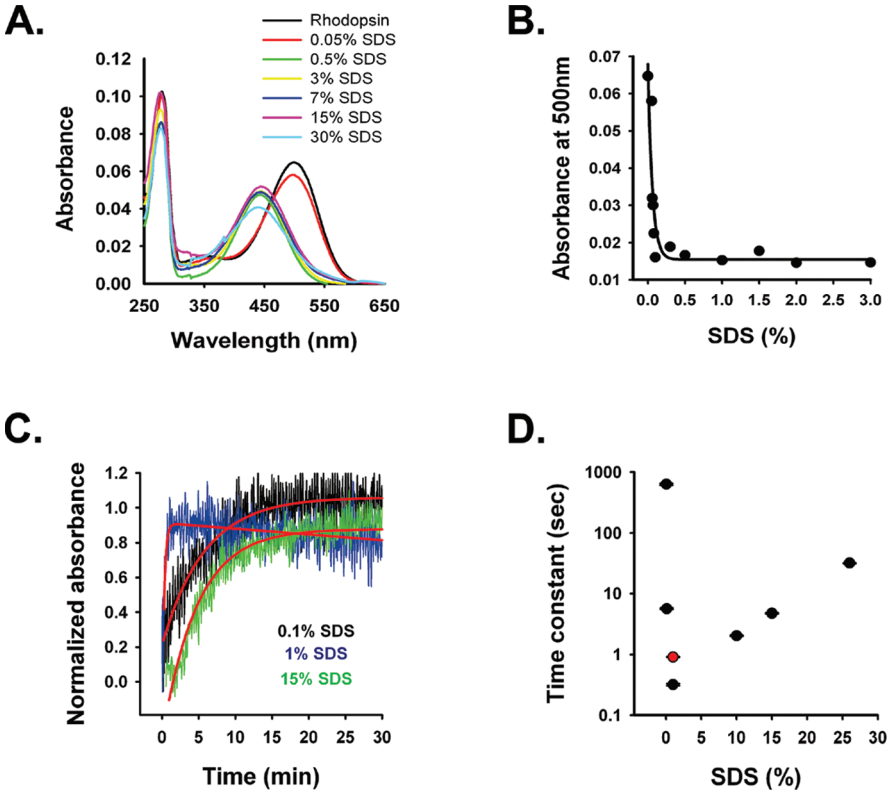

FIGURE 1: Stability of retinal−protein interactions. (A) Absorbance spectra of 1.5 μM rhodopsin alone (black line) and in different concentrations of SDS, as indicated in the figure, showing the shift in the 500 nm peak to 440 nm. (B) Plot showing decrease in absorbance at 500 nm with increasing SDS concentration up to 3%. (C) Stopped-flow kinetics following breakage of retinal−protein interactions for selected concentrations of SDS. Absorbance at 440 nm of rhodopsin denatured with SDS at concentrations of 0.1%, 1%, and 15% is plotted against time. Each curve was fitted to a monoexponential equation (see Methods). (D) Time constants obtained from the curve fittings of the absorbance kinetics obtained upon addition of 0.05%, 0.1%, 1%, 10%, 15%, and 26% SDS are plotted against each respective SDS concentration. To show reproducibility of the kinetics, a second data point for 1% SDS is included (red circle), which was obtained in a different measurement setup (see Methods).

The anisotropy decay was fitted with the model function:

$$r(t) = \sum_{i=1}^{n} \beta_i e^{-t/\Phi_i} \quad (4)$$

with β_i the amplitude and φ_i the time constant (correlation time) of the ith decay component.

RESULTS

Disruption of Retinal−Protein Interactions. SDS-induced disruption of secondary structure is described in detail in the accompanying paper (DOI 10.1021/bi100338e). To correlate these secondary structure changes with SDS-induced disruption of tertiary structure, we measured changes in the interaction between the chromophore retinal and rhodopsin. 11-*cis*-Retinal is covalently linked to Lys296 in the native dark state via a protonated Schiff base. Retinal binding contributes to the stability of rhodopsin and is important for its function. Retinal binding gives rise to a chromophore band in the absorption spectrum of rhodopsin at 500 nm and is used here as a tertiary structure probe. The absorption spectra of rhodopsin in the absence and presence of different amounts of SDS are shown in Figure 1A. The 500 nm peak characteristic of native rhodopsin shifts toward 440 nm with addition of increasing concentrations of SDS. A plot of the absorbance intensity at 500 nm as a function of SDS (Figure 1B) reveals a steep loss of 500 nm chromophore absorption, as the peak already begins to decrease in intensity on addition of 0.05% SDS and completely disappears on adding 0.1% SDS. The absorption maximum that forms at 440 nm (Figure 1A) instead is characteristic of a protonated Schiff base in solution devoid of specific protein contacts. This implies disruption of retinal−protein interactions on addition of relatively small concentrations of SDS. Over time, the 440 nm peak shifts to 380 nm, indicating formation of free retinal due to hydrolysis of the Schiff base (data not shown).

Fast Kinetics of the Disruption of Retinal−Protein Interactions. Only in the presence of 0.05% SDS, disruption of retinal−protein interactions occurs slowly, on the order of minutes. Above 0.05% SDS, formation of the 440 nm retinal band, indicative of rhodopsin denaturation, takes place in second and subsecond time scales. For these concentrations, we therefore measured the kinetics of the loss of native retinal−protein interactions using a stopped-flow apparatus (see Methods). An exponential increase in absorbance at 440 nm was observed for all SDS concentrations tested, and time traces are shown exemplary for some concentrations in Figure 1C. Time constants of the increase for all of the measurements made are plotted as a function of SDS concentration in Figure 1D. The loss of retinal−protein contacts proceeded drastically faster when going from 0.05% SDS (630 ± 20 s) to 1% SDS (0.32 ± 0.01 s) and indeed is the fastest at this concentration. Beyond 1% SDS, the time constant becomes slower with 2.04 ± 0.03 s at 10% SDS, 4.74 ± 0.06 s at 15% SDS and finally with 31.8 ± 0.4 s at 26% SDS. These results indicate that the helical bundle is most rapidly opened around 1% SDS as compared to other SDS concentrations allowing fast disruption of retinal−protein interactions and resulting in a protonated Schiff base devoid of protein contacts. The relatively fast time constant of denaturation at 1% SDS was

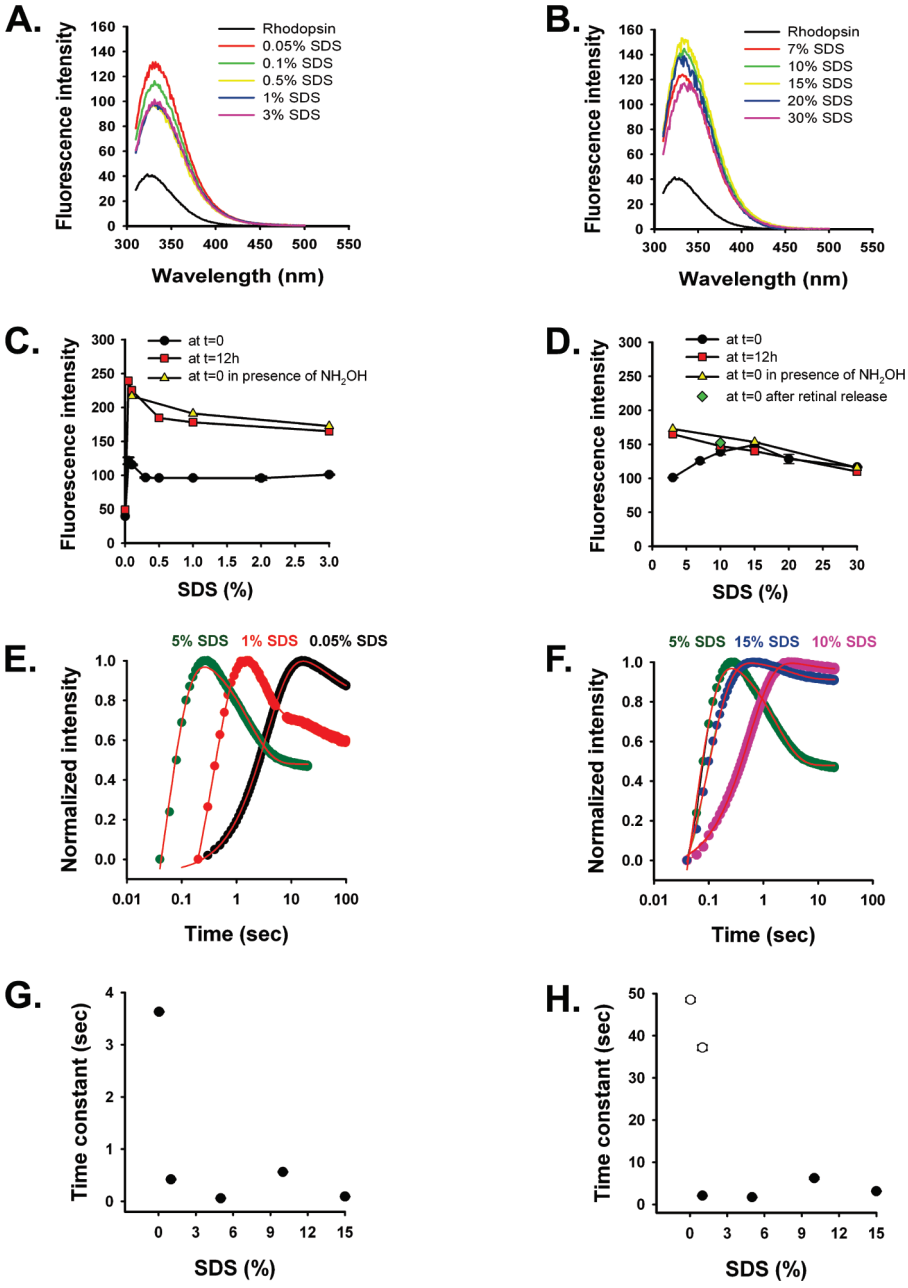

FIGURE 2: Changes in tryptophan fluorescence. Emission spectra of 1.5 μM rhodopsin upon titration with (A) 0.05%−3% SDS and (B) 7%−30% SDS in the wavelength range of 310−500 nm. Changes in fluorescence intensity at 330 nm at (C) 0.05%−3% SDS and (D) 7%−30% SDS concentrations immediately after its addition (t = 0), after incubation for 12 h (t = 12 h), immediately after its addition in the presence of 10 mM hydroxylamine (t = 0 in the presence of NH_2OH) and rhodopsin treated with 0.5% SDS in the presence of 10 mM hydroxylamine followed by increase in SDS concentration to 10% (t = 0 after retinal release). (E) Stopped-flow kinetics of fluorescence changes at SDS concentrations 5% and below. (F) Stopped-flow kinetics of fluorescence changes at SDS concentrations 5% and above. (G) Time constants of the fast tryptophan fluorescence increase as a function of SDS concentration. Time constants were obtained from a multiexponential fitting. The first component of each fit represents the monoexponential increase in fluorescence. (H) Time constants of the slow partial tryptophan fluorescence decrease as a function of SDS concentration. Except for 1% SDS all fluorescence decays were fitted monoexponentially. The data at 1% SDS were represented as a biexponential decay.

independently verified by a second measurement using 10 μM rhodopsin. This measurement yielded a time constant for the increase in absorbance at 440 nm of 0.91 ± 0.01 s (included in Figure 1D as a red circle).

Tertiary Structure Changes from Tryptophan Fluorescence. Unfolding of native helices and breaking of retinal−protein interactions are expected to result in changes in native tertiary interactions extending globally to disruption of the overall tertiary structure of rhodopsin. To characterize these structural changes, tryptophan fluorescence was employed as another internal tertiary structure probe. There are five tryptophan residues in rhodopsin, mainly located in close vicinity to the retinal chromophore. Their fluorescence in dark-adapted rhodopsin is quenched due to energy transfer to the retinal. The release of retinal, e.g., following light activation and decay of the activated metarhodopsin II species to free retinal and opsin, causes an increase in tryptophan fluorescence (*12*). Panels A and B of Figure 2 show changes in the fluorescence emission spectra of rhodopsin when titrated with SDS at low concentrations up to 3% and high concentrations up to 30%, respectively. Changes in fluorescence intensity at 330 nm as a function of SDS concentration are plotted in Figure 2C,D. There is a slight red shift in the wavelength of maximum emission from 330 to 335 nm when going from 0% to 30% SDS (Figure 2A,B). This shift indicates

exposure of tryptophan side chains to a polar environment consistent with rhodopsin denaturation and is not due to unspecific solvent-induced effects because free *N*-acetyltryptophan with increasing concentration of SDS shows a blue shift (data not shown).

The addition of 0.05% SDS causes a 3-fold increase in tryptophan fluorescence (Figure 2A,C). Further increases in SDS concentration resulted in lesser increases in fluorescence intensity as compared to the native state. Fluorescence in SDS remained essentially constant when comparing concentrations starting from 0.5% up to 2−3% SDS. The fluorescence intensity at these concentrations was still 2.5-fold greater than that of native rhodopsin. The result mirrors the relatively constant values observed in mean residue ellipticity (MRE) over the range 0.5%−3% SDS (DOI 10.1021/bi100338e). At SDS concentrations beyond 3%, illustrated in Figure 2D, there is a slight rise in fluorescence that maximizes at 15% SDS, where it is 1.5-fold higher as compared to the fluorescence at 3% SDS. Further increase in SDS up to 30% reverses this trend: a decrease in fluorescence is observed. To discriminate between protein and solvent-induced effects leading to these changes in tryptophan fluorescence, fluorescence of free *N*-acetyltryptophan was recorded over the same SDS concentration range of 0.05%−30%. A constant decrease in free *N*-acetyltryptophan fluorescence was observed from 0.05% to 3% SDS, and the pattern of change beyond 3% SDS and up to 30% SDS was the same as that seen with rhodopsin but only at a lower magnitude of intensity (data not shown). This shows that the initial increase in rhodopsin fluorescence on addition of 0.05% SDS is a protein-mediated effect.

We also probed changes in fluorescence as a function of time. Rhodopsin was incubated with SDS at various concentrations, and spectra were collected every 30 min. The fluorescence values at the end of 12 h of incubation time are plotted in Figure 2C,D (red squares). There was a drastic increase in fluorescence as compared to the results obtained at time zero. Even though noncovalent retinal−protein interactions are disrupted by the addition of SDS, we know that, initially, the retinal is still covalently linked to rhodopsin. We therefore suspected that this difference is due to hydrolysis of the protonated Schiff base. Hydrolysis occurs on adding SDS, which leads to the release of retinal over time (also see section Absorbance Spectroscopy, above). To test this hypothesis, we carried out SDS titrations in the presence of 10 mM hydroxylamine (NH_2OH) which cleaves the retinal Schiff base bond (*9*, *12*). In the presence of hydroxylamine the fluorescence measured immediately ($t = 0$, yellow triangles in Figure 2C,D) was identical to that observed in the absence of hydroxylamine only after 12 h ($t = 12$ h, red squares in Figure 2C,D). This observation indicates that the spike in fluorescence increase at very low SDS concentrations (0.05%) followed by the slow decrease in fluorescence at intermediate SDS concentrations (between 0.05% and 3%) is a protein-mediated effect. Retinal quenching simply dampens the absolute fluorescence values. A difference is observed for concentrations 3%−15%: here, in the presence of hydroxylamine and in its absence after 12 h, the same decreasing trend is followed, while in the absence of hydroxylamine at $t = 0$ there is an increase in fluorescence until the two curves meet. To rule out that this is due to inaccessibility of retinal to hydroxylamine at increased SDS concentrations, we confirmed hydrolysis using absorbance spectroscopy. Hydroxylamine reaction with the Schiff base results in formation of retinal oxime which gives a characteristic absorbance maximum at 360 nm (*13*). This peak was observed when rhodopsin in 10% SDS was incubated with hydroxylamine, confirming that retinal is hydrolyzable under these conditions (data not shown). It was also observed that retinal hydrolysis occurred over time when rhodopsin is treated with 10% SDS (data not shown). To further confirm that the lack of increase in fluorescence in the presence of hydroxylamine at SDS concentrations greater than 3% is not due to retinal quenching, retinal was first removed by adding 0.5% SDS to rhodopsin in the presence of hydroxylamine, and then the SDS concentration was increased to 10%. The fluorescence counts of this experiment (shown as a green diamond in Figure 2D) was found to overlap with fluorescence counts of rhodopsin in 10% SDS at $t = 0$ and $t = 12$ and that at $t = 0$ in the presence of NH_2OH. Thus, the presence or absence of covalently linked retinal has no effect on the fluorescence of denatured rhodopsin in the presence of SDS concentrations in excess of 3% (Figure 2D), while at lower SDS concentrations, the presence of retinal quenches tryptophan fluorescence of rhodopsin.

Fast Kinetics of Tertiary Structure Changes from Tryptophan Fluorescence. To complement the measurements of tertiary structure changes as measured by tryptophan fluorescence at steady state, we also carried out stopped-flow experiments of denaturation. The results are shown in Figure 2E−H. In each case, we observed multiexponential kinetics of the tryptophan fluorescence transients induced by the addition of SDS. At each SDS concentration, there is a fast initial rise in fluorescence followed by a partial decrease (Figure 2E,F). The time constants of the rise and decay of the fluorescence transient as a function of SDS concentration are plotted for the initial rise in Figure 2G and for the subsequent partial decrease in Figure 2H. The SDS dependence of the end amplitudes of the tryptophan fluorescence time traces mirrors the SDS dependence of the steady-state fluorescence data presented in Figure 2C,D. The kinetics of the tryptophan fluorescence rise and decay components show a similar SDS dependence, with the slowest time constants observed at low concentrations and fast time constants observed above 1% SDS. It seems that below 1% SDS the kinetic processes leading to tertiary structure changes upon rhodopsin denaturation are different from those observed above 1%. This is indicated by the two fluorescence decay components observed at 1%, where probably a mixture of the two regimes exists. At both 0.05% and 1% SDS a slow time constant for the tryptophan fluorescence decay around 40 s exists. At 1% SDS an additional fast decay time constant below 10 s with approximately 75% of the total amplitude appears, agreeing with the decay time constant obtained above 1% SDS.

Tertiary Structure Changes from Cysteine Reactivity. Reactivity of cysteine residues was used as an additional global tertiary structure indicator. The native cysteine residues in rhodopsin are fortuitously distributed across the entire structure, shown as blue circles in Figure 3A. Accessibility of cysteine residues was probed using the cysteine derivatizing agent, 4,4′-dithiodipyridine (4-PDS). 4-PDS reacts with the accessible free sulfhydryl groups of cysteines releasing stoichiometric amounts of 4-thiopyridone which has an absorption maximum at 323 nm (*10*). Of the six free cysteines in rhodopsin, only two of them, depicted by blue arrows in Figure 3A, can be derivatized in the dark state whereas all six of them can be derivatized upon loss of 11-*cis*-retinal on light activation (*14*). Rhodopsin (1.5 μM) was treated with different concentrations of SDS and then reacted with a 25-fold excess of 4-PDS. The reaction was followed spectrophotometrically by monitoring the increase in absorbance at

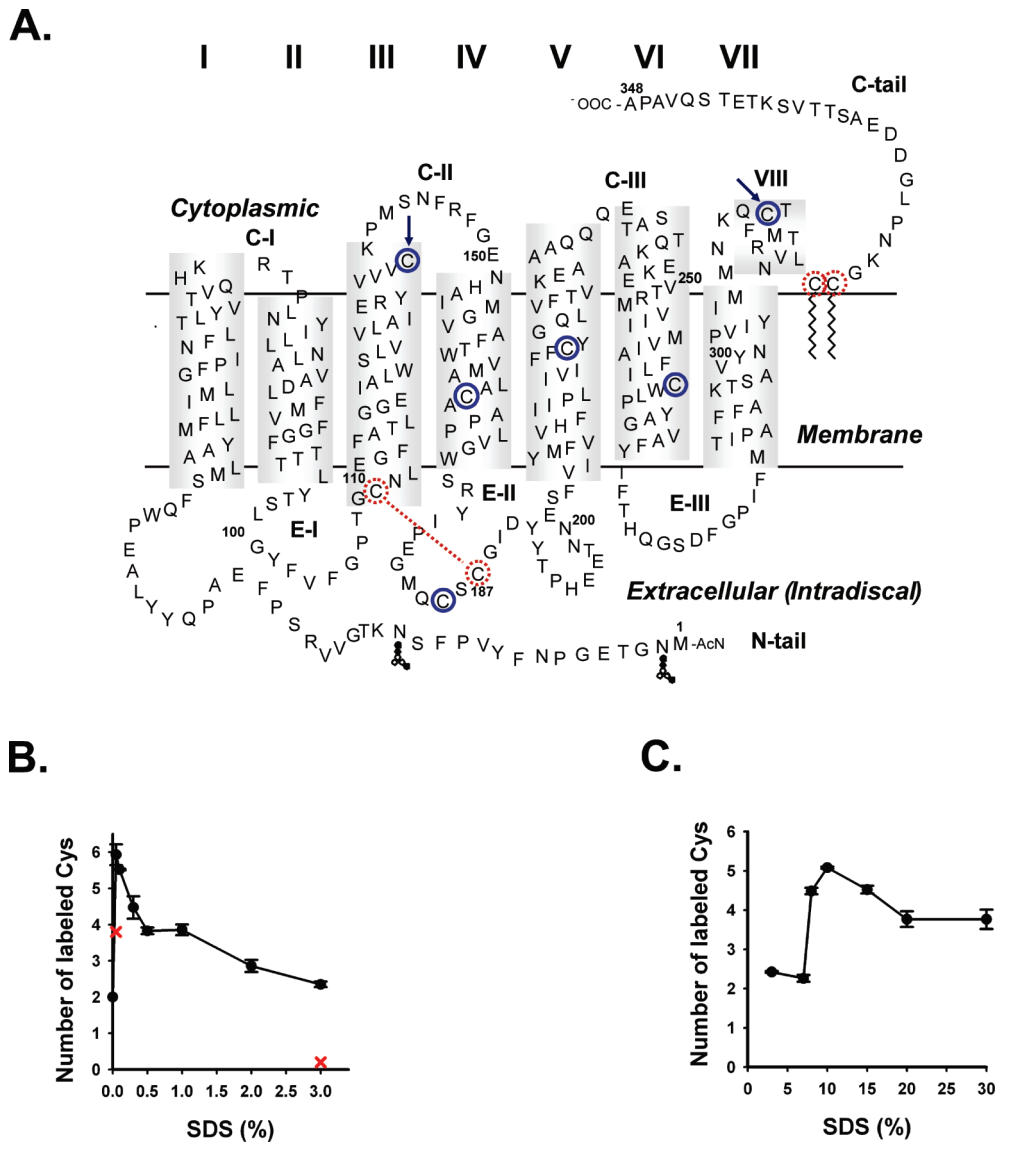

FIGURE 3: Changes in cysteine accessibility on SDS addition. (A) Secondary structure representation of rhodopsin showing the six cysteines that are reactive in the light-activated Meta II state of rhodopsin (blue solid circles). The positions of C140 and C316 are shown by blue arrows. Cysteines at positions 110 and 187 are engaged in a disulfide bond, and cysteines at positions 321 and 323 are palmitoylated; they are therefore not reactive. These nonreactive cysteines are shown as red dotted circles, and the disulfide bond is indicated as a red dotted line. (B) Number of reactive cysteines against SDS concentration ranging from 0.05% to 3% is plotted. The reactivity of cysteines in the C140S/C316S mutant is shown as crosses at 0.05% and 3% SDS. (C) Number of cysteines accessible at higher SDS concentrations from 3% to 30% are shown.

323 nm (Methods). Figure 3B shows the variation in the number of cysteines being labeled with 4-PDS with increasing SDS concentrations. Denaturation of rhodopsin by 0.05% and 0.1% SDS resulted in all six cysteines becoming reactive to 4-PDS (Figure 3B). This indicates opening of the helical bundle of rhodopsin on SDS denaturation consistent with the tryptophan fluorescence data (Figure 2A). Subsequent increases in the SDS concentration decrease the accessibility of the cysteines to only two in the SDS concentration range of 3%−7%, as illustrated in Figure 3B,C.

In order to identify the two cysteines that are accessible at the elevated SDS concentrations, we replaced C140, in the second cytoplasmic loop, at the interface of the TM and the cytoplasmic domain, and C316, in the fourth cytoplasmic loop, each with serine residues by site-directed mutagenesis. For reference, the locations of these cysteines in the rhodopsin structure are shown by blue arrows in Figure 3A. The C140S/C316S double mutant was denatured with 3% SDS, and the reactivity of the remaining four cysteines was assessed using 4-PDS, as described above for the wild type. At low concentrations of SDS, four cysteines were labeled as expected (shown as a red cross in Figure 3B). In the presence of 3% SDS, no cysteines were labeled in the mutant (red cross in Figure 3B). The absence of a 323 nm peak for the SDS-denatured C140S/C316S double mutant at 3% SDS indicates that the two cysteines that were derivatized by 4-PDS in 3% SDS in the wild type are C140 and C316. This result points to the formation of a compact intermediate state at elevated SDS concentrations (around 3%), where only surface-exposed cysteines are accessible.

At SDS concentrations greater than 7%, there is again a dramatic increase in cysteine reactivity resulting in five reactive cysteines at 10% SDS (Figure 3C). This observation is in concord with the increase in tryptophan fluorescence counts of rhodopsin treated with SDS in the range of 3%−10% (Figure 2D). However, further increases in SDS concentration up to 30% decrease cysteine reactivity toward 4-PDS where four cysteines remain reactive (Figure 3C). This decrease in cysteine reactivity is again coherent with the decrease in tryptophan fluorescence intensity

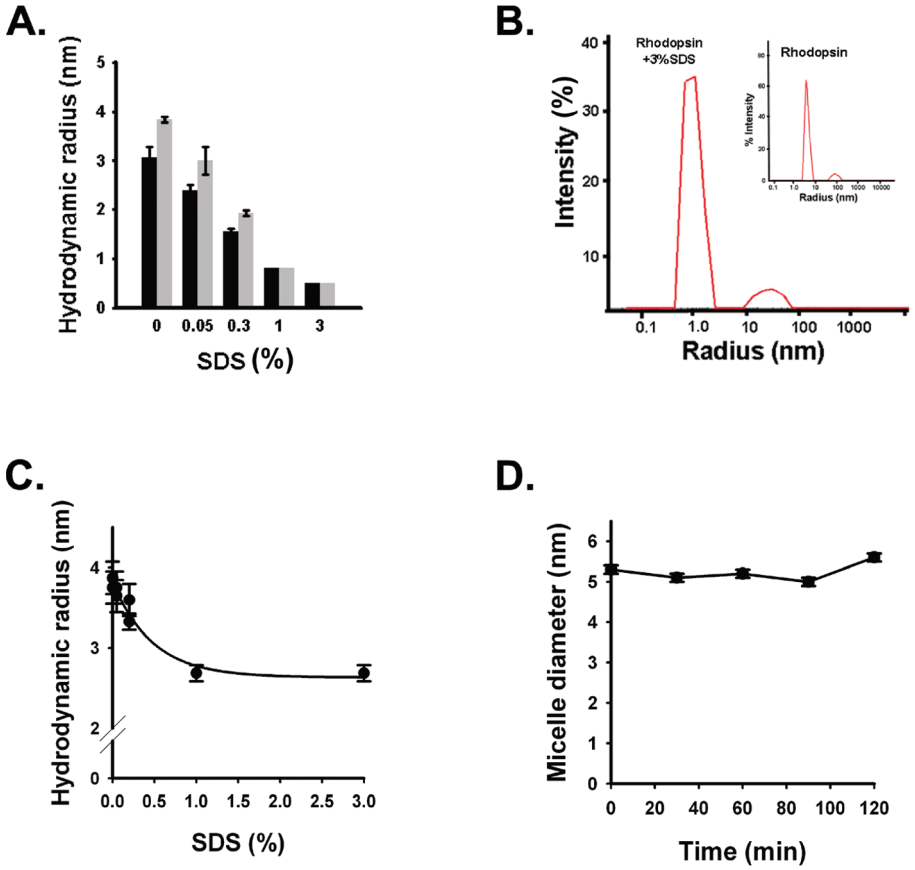

FIGURE 4: Probing rhodopsin aggregation by dynamic light scattering and fluorescence depolarization. (A) Decrease in hydrodynamic radius (R_h) of mixed DM−SDS micelle with (gray bars) and without (black bars) rhodopsin at increasing concentrations of SDS. (B) Only one major peak at R_h = 0.4 nm was observed when 1.5 μM rhodopsin was treated with 3% SDS. No other peak was observed. The inset shows that the hydrodynamic radius of rhodopsin in DM micelles is 4 nm. (C) Decrease in hydrodynamic radius (R_h) of mixed DM−SDS micelle containing rhodopsin at increasing concentrations of SDS (0.05%−3%) as obtained from fluorescence depolarization. (D) Stability of rhodopsin mixed micelle size at 1% SDS as a function of time.

observed in the SDS concentration range of 15%−30%. The coherence of the SDS concentration dependent changes in cysteine accessibility between 7% and 20% SDS with the tryptophan intensity changes suggests a specific SDS-driven protein structural change in this SDS range.

Determination of the Size of Intermediates during SDS Denaturation. The evidence described above indicates that cysteine and tryptophan residues become buried over the range 0.05%−3% SDS. We ruled out aggregation as a possible cause for this effect in the accompanying paper (DOI 10.1021/bi100338e). To see if there are any changes in the size of denatured rhodopsin that may explain these results, this SDS concentration range was further investigated by dynamic light scattering and fluorescence depolarization experiments.

(*1*) *Dynamic Light Scattering*. SDS was titrated into 2 mM sodium phosphate buffer containing 0.05% DM as a control and into the same buffer containing rhodopsin (Figure 4A). The size of the DM micelles in sodium phosphate buffer is estimated to be 3 nm (hydrodynamic radius), and that with rhodopsin is observed to be 4 nm as shown by black and gray bars, respectively, in Figure 4A. SDS molecules have the same chain length as DM molecules. Therefore, addition of SDS to DM micelles results in their entering into the DM micelles and forming mixed micelles (*15*). The size of such mixed micelles was first tested in the absence of rhodopsin. A decrease in size from 3 to 0.4 nm was observed when 3% SDS was added to 0.05% DM (black bars in Figure 4A). These values were calculated after taking into account viscosity coefficients of SDS-titrated buffer solutions. The viscosity, η, of 0.05%−2% SDS solutions was measured to be 1 cP (same as that of water), and that of 3% SDS solution was determined to be 1.27 cP. The hydrodynamic radius of rhodopsin in DM micelles was observed to decrease from 4 nm in the absence of SDS to 0.4 nm at 3% SDS (gray bars in Figure 4A). Since SDS is an anionic detergent, its aggregation number of 62 at its critical micellar concentration (*16*) is smaller compared to that of DM, which is 98 (*17*). Hence, the decrease in mixed micellar size on increasing SDS concentration in the lower SDS concentration range indicates that the DM molecules are increasingly getting replaced by SDS molecules both in the absence and in the presence of rhodopsin. Figure 4B shows a peak at 0.4 nm for rhodopsin micelles in 3% SDS. A small peak of very low intensity compared to the peak at 0.4 nm appears, but this peak is also seen for rhodopsin alone in the absence of SDS (Figure 4B and inset of Figure 4B). This peak may originate from impurities in the solution since it was not filtered before the experiment. This is because when sodium phosphate buffer containing DM was filtered, highly intense peaks of large size were seen (data not shown).

(*2*) *Fluorescence Depolarization*. To corroborate the findings from dynamic light scattering, we also inferred the size of the rhodopsin micelles by using the slowest rotational correlation time of the fluorescence depolarization experiments. This time constant describes the tumbling of the whole micelles and can thus be used to calculate the size of the rhodopsin micelles at

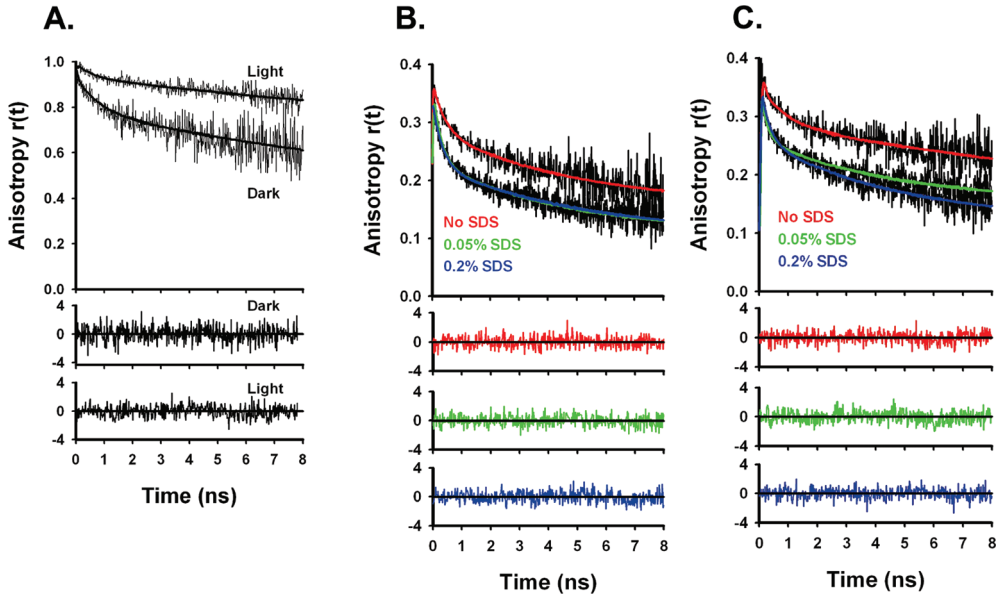

FIGURE 5: Probing rhodopsin surface dynamics by fluorescence depolarization. (A) Anisotropy decay curves of fluorescein attached to C316 in H8 measured before and after light activation of rhodopsin in 0.05% DM micelles and phosphate buffer, pH 6, 20 °C. The anisotropy curves are normalized and displayed on a logarithmic scale. (B) Change in the anisotropy decay curve of fluorescein attached to C316 in H8 after addition of 0.05% (green) and 0.2% (blue) SDS to rhodopsin in 0.05% DM micelles and phosphate buffer, pH 7.5, 20 °C. (C) Change in the anisotropy decay curve of fluorescein attached to C316 in H8 after addition of 0.05% (green) and 0.2% (blue) SDS to rhodopsin in 0.05% DM micelles and phosphate buffer, pH 6.0, 20 °C. The residuals of the fits according to eq 4 are shown. Curves obtained in the absence of SDS are shown in red in subfigures B,C.

varying SDS concentrations. To rule out interference of SDS micelles without rhodopsin at increasing SDS concentration, masking the real size of the rhodopsin SDS micelles, a fluorescent reporter group was attached to the rhodopsin molecule. This allows us to monitor only those micelles which contain rhodopsin. In the absence of SDS a hydrodynamic radius of 3.7 nm was calculated from the rhodopsin micelle rotational correlation time using the following relationship of the slowest rotational correlation time (Φ_3) and the volume of the rotator (V), $\Phi_3 = \eta V/k_B T$, assuming a sphere-like shape of the mixed micelle. This value is in very good agreement with the radius of 4 nm obtained from the light scattering measurements. With increasing SDS concentrations, however, the radii obtained from the light scattering experiments and from fluorescence depolarization diverge (Figure 4A,C). The hydrodynamic radius of the rhodopsin micelles levels off between 1% and 3% SDS at a value of 2.6 nm (Figure 4C), while the radii obtained from the light scattering experiments reach the values for SDS micelles in the absence of rhodopsin for SDS concentrations above 1% SDS. This is because light scattering cannot differentiate between rhodopsin-containing and empty micelles. With increasing SDS concentrations more empty micelles are present in comparison to rhodopsin-containing micelles, thus masking the real value for the latter.

Rotational correlation time was also followed as a function of time as shown in Figure 4D. No time-dependent changes in micelle size were observed within 2 h after 1% SDS addition.

Disruption of Surface Tertiary Structure from Time-Resolved Fluorescence Depolarization. Tryptophan fluorescence and cysteine accessibility studies suggest rhodopsin unfolding states that range from an opening of the helical bundle at low SDS concentrations of 0.05% to a compact form at elevated SDS concentrations of 3% (and again at 30%). Dynamic light scattering and fluorescence depolarization results also showed a decrease in hydrodynamic radius of denatured states at 3% SDS. However, secondary structure is clearly disrupted, indicating that some parts of the protein must become more flexible while the others contribute to the compact core. The cysteine reactivity studies indicate that these more flexible parts are located at the protein surface. We therefore decided to investigate in more detail how protein surface segments at the membrane/water interface respond to SDS. To do so, we measured the real-time dynamics at the cytoplasmic surface of rhodopsin using time-resolved fluorescence depolarization. The fluorescence reporter group fluorescein was covalently attached to C316 (*18*) in the middle of a helical stretch, helix-8 (H8), that runs parallel to the cytoplasmic surface and connects the membrane spanning part of rhodopsin with the long C-terminal tail. Because of its amphipathic nature, H8 is sensitive not only to changes in protein structure but also to changes in the lipid or detergent environment (*19*−*21*). The dynamics of H8 was investigated at pH 6 and 7.5 at 0% SDS in the dark- and light-activated state of rhodopsin/DM micelles and compared to 0.05%, 0.2%, 1%, and 3% SDS added to rhodopsin in the dark. The analysis of the anisotropy decay curves (Figure 5) and the assignment of the decay components to (i) the dynamics of the dye, (ii) the flexible segment the dye is bound to, and (iii) the tumbling of the whole micelle were performed as described previously (*18*, *22*). The goodness of the fit and number of decay components were judged from the reduced χ^2 values of the fit. The anisotropy data, fits, and residuals of the fits are presented in Figure 5. The anisotropy data were fitted with three-exponential decay components. The fastest anisotropy decay component with about 100−300 ps was attributed to the dynamics of the bound fluorescent dye. The second decay component was assigned to the real-time dynamics of H8. The amplitude of the third decay component describes the steric restriction of H8 mobility due to the surrounding detergents and the protein surface. As already reported (*23*), light activation of rhodopsin leads to an increased steric restriction of H8 movement (Figure 5A), as seen by the increase in final anisotropy. As shown in Figure 5B,C, the overall steric restriction of H8 movement by

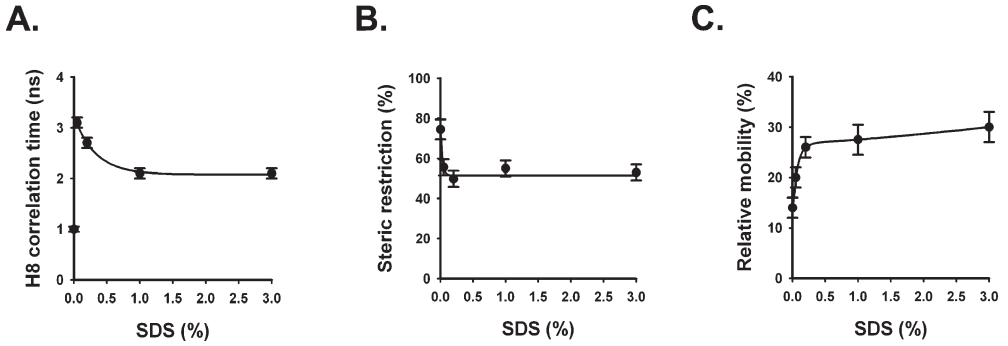

FIGURE 6: SDS dependence of H8 dynamic properties. (A) H8 correlation time as a function of SDS concentration. (B) Steric restriction of H8 mobility as a function of SDS concentration. (C) H8 mobility (amplitude of H8 anisotropy decay component) as a function of SDS concentration.

the surrounding protein elements decreases dramatically upon addition of minute amounts of SDS (0.05%), as seen from the decreasing amplitude of final anisotropy. This corresponds to the similar abrupt decrease in helicity as observed by circular dichroism, the burst of tryptophan fluorescence, and the increase in cysteine accessibility at 0.05% SDS. The interpretation of an initial opening of the helix bundle at these low SDS concentrations based on the increase in cysteine accessibility fits with the reduced interaction of H8 with its surroundings.

A closer look at the SDS concentration dependence of the H8 dynamics parameters at pH 6 (Figure 6) shows that multiple conformational changes of H8 occur upon SDS addition. At 0.05% SDS the diffusional correlation time of H8 slows down from 0.8 ± 0.1 to 3.1 ± 0.1 ns (Figure 6A) and the steric restriction of H8 movement drops by about 30% (Figure 6B). After the initial slowdown in H8 real-time dynamics, the H8 dynamics becomes faster again with a half-maximum value of 0.33 ± 0.06% SDS and remains constant up to 3% SDS with a correlation time of about 2 ns. The half-maximum value for the first increase in H8 relative mobility (conformational space) is 0.14 ± 0.05% SDS, while a further but less pronounced increase in mobility was observed between 1% and 3% SDS (Figure 6C). This behavior is reminiscent of the biphasic decrease in cysteine accessibility. These results also support the idea that protein surface elements become more flexible between 1% and 3% SDS while others within the membrane region probably form the compact core.

DISCUSSION

Here, we report the first biophysical characterization of unfolded states of the mammalian membrane protein rhodopsin. In particular, we studied SDS-induced unfolding of rhodopsin because in the accompanying paper (DOI 10.1021/bi100338e) we show that this denaturant causes maximal unfolding of rhodopsin without aggregation. SDS has been commonly used as a denaturant for both membrane proteins (*24*−*27*) and soluble proteins (*28*−*33*). It was shown that the modes of unfolding depend on the SDS concentration range used (*34*, *35*). In the accompanying paper (DOI 10.1021/bi100338e) we deduced four denaturation stages based on CD measurements, which correlate with the types of SDS micellar structures expected at different concentrations (Figure 8 of the accompanying paper). These are DM/SDS mixed micelles (stage 1, 0.05−0.3% SDS), SDS spheres (stage 2, 0.3−3% SDS), SDS spheres/cylindrical mixed micellar states (stage 3, 3−15% SDS), and predominantly cylindrical micelles (stage 4, above 15% SDS). [Note that the use of the word "stages" does not imply a temporal progression and is used in this context only to describe the respective conformational states observed at a particular SDS concentration range.] While stages 1 and 2 are characterized by a gradual loss in membrane protein helicity of up to ~19%, stage 3 includes the formation of non-native helices, a well-known property of SDS when a very large number of detergent molecules interact with the membrane protein and SDS is going from spherical to cylindrical shape. In stage 4, a ~40% decrease in helical content characterizes the largely unfolded states of rhodopsin induced by SDS cylindrical micelles that aggressively unfold the membrane protein at 30% SDS. The identification of these four denaturation stages is corroborated by the characterization of tertiary structure presented in this paper. We utilized five independent probes, retinal−rhodopsin interaction, cysteine reactivity toward 4-PDS, tryptophan fluorescence, hydrodynamic radius of denatured states, and real time dynamics of the amphiphatic H8 at the cytoplasmic rhodopsin surface.

In stage 1 of SDS denaturation, at very low SDS concentrations (0.05%), initial opening of the helical bundle leads to an instantaneous increase in tryptophan fluorescence and cysteine accessibility in the protein core, while retinal−rhodopsin interactions only begin to be disrupted. The tryptophan fluorescence increase takes place within seconds. In contrast, the partial loss of retinal−protein interactions occurs very slowly at 0.05% (in the minute time range), indicating that there are not sufficient SDS molecules present at these concentrations to cause the breakage of native retinal−protein contacts. However, at 1% SDS, the loss of retinal contacts occurs very fast; in fact, it reaches a peak indicating that at this stage optimal amounts of SDS are available to carry out this process. Beyond 1% SDS, i.e., at 10%, 15%, and 26% SDS, the rates of the reaction slow down again, indicating that the formation of cylindrical micelles at these concentrations of SDS is retarding the disruption of protein contacts including retinal−protein contacts. Thus, in stage 1 (at 0.05% SDS) there is a fast initial opening of the helical bundle, which is characterized by an increase in tryptophan and cysteine accessibility. This initial opening should be viewed as a softening of the helix bundle because it allows only partial loss of retinal−protein contacts leading to a slow "full" opening of the helical bundle (Figure 7A).

The small number of SDS molecules present at these low concentrations of SDS (0.05%) leads to changes at the cytoplasmic protein surface as evidenced by a decrease in steric restriction of H8 mobility and a slowdown in H8 motion. At such very low SDS concentrations it was suggested that H8 adopts a β-sheet-like structure (*20*). Structural changes that involve H8 may have long ranging effects due to the conserved NPxxY(x)F motif in

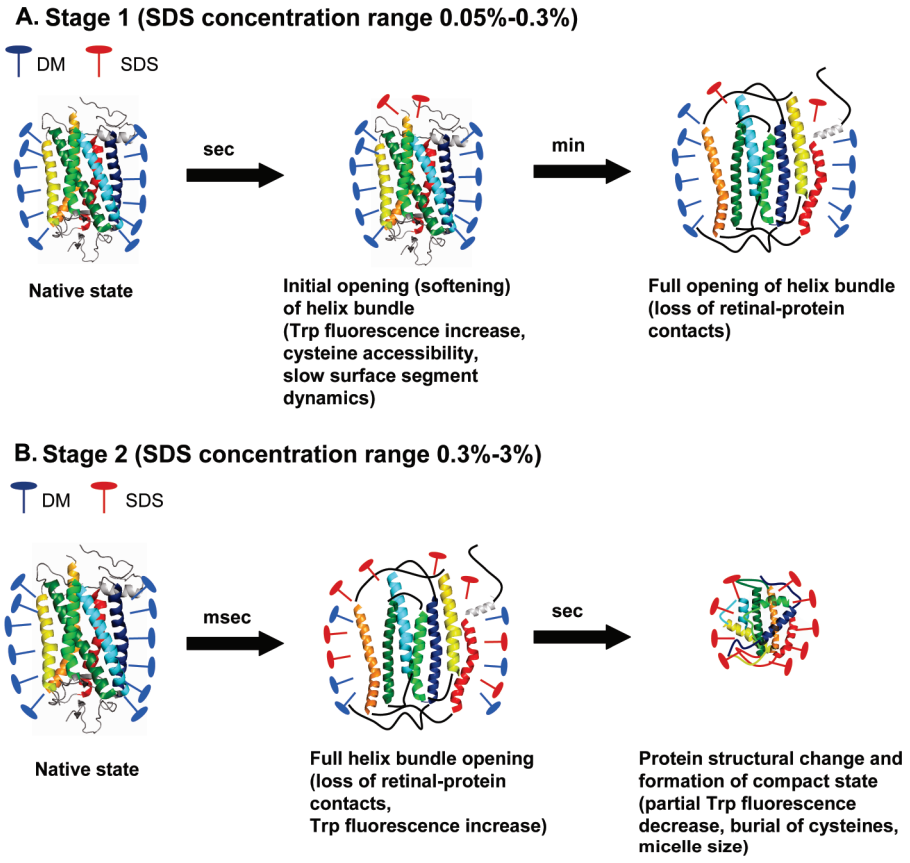

FIGURE 7: Model depicting structural changes in rhodopsin in stages 1 and 2 of SDS denaturation. (A) Stage 1 represents addition of 0.05% SDS to rhodopsin whereby an initial slow opening of helical bundle on a time scale of seconds occurs. This is followed by complete opening of the bundle on a time scale of minutes. (B) Stage 2 refers to denaturing concentration of SDS beyond 0.05% up to 3% whereby an opening of the helical bundle occurs in milliseconds followed by structural changes in rhodopsin leading to formation of a compact state is seen on a second time scale.

transmembrane helix 7 preceding cytoplasmic H8. A decrease in steric restriction of H8 mobility, for instance, was also seen in dark rhodopsin at high pH values and low temperature, conditions which shift the equilibrium between the active receptor state Meta II and its inactive precursor state toward the latter (*18*). From the seven-helix transmembrane protein bacteriorhodopsin a double mutant is known which displays long-range effects between the cytoplasmic end of transmembrane helix 7 and the retinal binding pocket (*36*, *37*), supporting the idea that subtle changes at this C-terminal region may affect properties of the protein core. Surface charge changes may also contribute. Conformational changes of membrane protein surface elements were shown to be dependent on surface charge changes (*18*, *38*).

A similar trend in SDS dependence is also seen in measurements of cysteine reactivity toward 4-PDS, which has been previously utilized to study conformational changes in rhodopsin (*39*, *40*). Here, this reaction was exploited to investigate tertiary structure changes under SDS denaturing conditions. While interpretation of cysteine accessibility results under denaturing conditions is qualitative due to possibilities such as disulfide exchange reactions in unfolded states and effects of the hydrophobic environment on the molar extinction coefficient of 4-PDS, these factors are expected to influence the results mostly at high SDS concentrations beyond 3%. At low concentrations of 0.05% and 0.1% SDS, all six free cysteines in rhodopsin react with 4-PDS compared to only two cysteines reacting in the native state. This may be triggered by perturbation of retinal interactions with rhodopsin at low SDS concentrations. The initial opening of the helical bundle is accompanied by an increase in accessibility of the cysteine side chains to 4-PDS and an increase in tryptophan fluorescence. This supports the notion that the initial opening or softening of the helical bundle, probably mediated by surface-induced long-range effects, is the first stage of denaturation of tertiary structure by SDS. This interpretation is further corroborated by the decrease in steric hindrance of H8 mobility, which is expected when the helix bundle opens up and leaves more conformational space for individual protein elements especially at the protein surface.

In the second stage, in the range of 0.05%−3% SDS, the increase in SDS concentrations up to 0.5% decreases the tryptophan fluorescence counts, which then remain constant up to 3% SDS. Cysteine reactivity shows a continuous decrease, which plateaus at two reactive cysteines in the presence of up to 3% SDS. The tryptophan fluorescence kinetics show a biphasic behavior with fast increase and partial decrease for all SDS concentrations used. In contrast to stage 1, the kinetics of tryptophan fluorescence increase coincide with the kinetics of the disruption of native retinal contacts (0.4 and 0.3 s at 1% SDS, respectively), indicating that the amount of SDS molecules is sufficient to break native retinal−protein contacts very fast, leading to a full opening of the helix bundle. The kinetics of the partial fluorescence decrease is somewhat slower with values in the lower second range. Taking the development of a plateau between 0.5% and 3% SDS for both tryptophan fluorescence and cysteine accessibility into account, we associate the fluorescence decay kinetics in the second time range with a protein structural change leading to the burial of the cysteines (Figure 7B). These changes in the protein core are paralleled

by faster H8 correlation times and increased H8 mobility at the rhodopsin surface, probably due to the re-formation of a helical structure of H8 at higher SDS concentrations (*20*). This constitutes the second stage of unfolding. Several lines of evidence indicate that this second stage constitutes a stable compact intermediate state during SDS denaturation. The observed decreases in cysteine reactivity and tryptophan fluorescence from 0.05% to 3% SDS can be explained by the burial of four of the six cysteines and one or more of the tryptophan side chains during SDS denaturation in a compact intermediate state. In order to identify the cysteines that are getting buried and better characterize this intermediate, we carried out mutagenesis experiments whereby two cysteines, C140 and C316, near the cytoplasmic domain were mutated to serines. It is expected that denaturation will occur more favorably near the extramembranous domain causing the cysteines at this surface to be more accessible to derivatizing agents. The C140S/C316S double mutant showed no reactivity toward 4-PDS at 3% SDS, confirming that the two cysteines that remain reactive at 3% SDS in the wild type are indeed C140 and C316, located at the rhodopsin surface. The burial of the other cysteines could be due to either formation of a compact intermediate or masking by solvent molecules, SDS micelles in this case. Light scattering and fluorescence depolarization results strongly support the possibility of formation of a compact intermediate during the second stage of SDS unfolding. The hydrodynamic radius of the DM micelle with rhodopsin was estimated to be 4 nm. With increasing concentrations of SDS the radius decreases up to a value of 2.6 nm in 3% SDS. This indicates that SDS molecules are displacing the DM molecules, thus surrounding rhodopsin in its unfolded state. Generally, for soluble proteins the hydrodynamic size increases on denaturation due to unfolding of the native structure. The contrary observed here indicates the possibility of formation of a compact intermediate which is surrounded by SDS molecules. Thus, at the second stage of unfolding, a compact protein core with an increased flexibility at the cytoplasmic surface is formed (Figure 7B).

SDS concentrations between 3% (100 mM) and 15% (500 mM) form the third stage of unfolding as the increase in aggregation number of SDS beyond 6% (200 mM) leads to structural transition of SDS micelles from spherical to cylindrical (*41*). The effect of a very large number of SDS molecules interacting with rhodopsin can be clearly seen in our CD experiment where there is an increase in the magnitude of MRE at 222 nm at 10% SDS to a value close to the native state, indicating that SDS is inducing nonnative helices, a well-known property of SDS (see accompanying paper, DOI 10.1021/bi100338e). However, these helices clearly lack interhelical interactions within the cylindrical SDS micelles, as an increase in cysteine accessibility and tryptophan fluorescence is observed as compared to the previous stage. The time dependence of the fluorescence counts and the analysis of fluorescence after treatment with hydroxylamine indicate that the retinal also lacks interactions with the rest of the protein that would lead to tryptophan quenching. Above 5% SDS, the kinetics of the formation of the 440 nm denatured rhodopsin species, indicative of the loss of retinal−protein contacts, becomes again slower than the internal protein conformational changes as measured by tryptophan fluorescence. The formation of cylindrical micelles at these concentrations of SDS is retarding the breakage of retinal−protein contacts probably due to the formation of stabilizing nonnative protein structures.

The fourth stage of unfolding at SDS concentrations beyond 10% is characterized by a drastic disruption of helical structure: an ~40% decrease in MRE at 222 nm at 30% SDS (1 M) is observed (see accompanying paper, DOI 10.1021/bi100338e). This corresponds approximately to a 45% decrease in helical content as estimated using the CDPro software (*42*). This is consistent with so-called "mode 2" unfolding in which SDS cylindrical micelles wrap around the protein and aggressively unfold it (*34*, *35*). However, despite the large degree of unfolding, we also see a decrease in fluorescence and in cysteine accessibility, where only four cysteines are reactive in the range of 15%−30% SDS as compared to five cysteines in stage 3. Therefore, it is likely that residual structure formed in the largely unfolded state of rhodopsin induced by 30% SDS is localized at a site that buries two cysteines and one or more tryptophan residues.

The possibility of formation of a folding core during folding of rhodopsin has been considered in the long-range interaction model (*2*). Computational modeling of denaturation of rhodopsin suggests that TM helices in rhodopsin do not unfold independently of each other, and at the end of the unfolding process a rigid region remains that consists of residues from EC loops and TM helices (*3*). Our findings of a compact intermediate during denaturation of rhodopsin can be considered as preliminary evidence toward the presence of a folding core during its initial folding stages. However, correlating our studies of SDS denaturation with that of the above folding model will require identification of the location of the residual structure and its characterization in the future.

In summary, here we have characterized the SDS denaturation of rhodopsin and interpreted the results in light of changes in SDS micellar structures with increasing concentrations of SDS. Evidence from light scattering suggests that SDS initially replaces DM molecules, initiating the formation of the environment needed to disrupt rhodopsin secondary and tertiary structure. We show by using absorbance and fluorescence spectroscopy as well as stopped-flow measurements that a softening and initial opening of the helical bundle of rhodopsin, followed by disruption of retinal−protein interactions with full opening of the helix bundle, are the first two steps in denaturation, the kinetics of which depend on the amount of SDS used. Fluorescence and cysteine reactivity measurements indicate burial of tryptophans and cysteine side chains in a compact intermediate. Compactness in overall size is also shown by light scattering and fluorescence depolarization. In contrast, flexibility of the cytoplasmic surface increases.

ACKNOWLEDGMENT

We thank Dr. William Furey, VA Medical Center, University of Pittsburgh, for access to the DynaPro instrument. We also thank Boris Repen and Peter Lachmann for help with data acquisition. Finally, we thank Dr. Catalina Achim and Jing Kong, Carnegie Mellon University, and Dr. Michael Trakselis, University of Pittsburgh, for help in recording stopped-flow absorbance and fluorescence measurements, respectively.

REFERENCES

1. Popot, J. L., and Engelman, D. M. (1990) Membrane protein folding and oligomerization: the two-stage model. *Biochemistry 29*, 4031–4037.
2. Klein-Seetharaman, J. (2005) Dual role of interactions between membranous and soluble portions of helical membrane receptors for folding and signaling. *Trends Pharmacol. Sci. 26*, 183–189.
3. Rader, A. J., Anderson, G., Isin, B., Khorana, H. G., Bahar, I., and Klein-Seetharaman, J. (2004) Identification of core amino acids stabilizing rhodopsin. *Proc. Natl. Acad. Sci. U.S.A. 101*, 7246–7251.

4. Tastan, O., Yu, E., Ganapathiraju, M., Aref, A., Rader, A. J., and Klein-Seetharaman, J. (2007) Comparison of stability predictions and simulated unfolding of rhodopsin structures. *Photochem. Photobiol. 83*, 351–363.
5. Park, P. S., Palczewski, K., and Muller, D. J. (2008) Mechanical properties of bovine rhodopsin and bacteriorhodopsin: possible roles in folding and function. *Langmuir 24*, 1330–1337.
6. Oprian, D. D., Molday, R. S., Kaufman, R. J., and Khorana, H. G. (1987) Expression of a synthetic bovine rhodopsin gene in monkey kidney cells. *Proc. Natl. Acad. Sci. U.S.A. 84*, 8874–8878.
7. Moller, M., and Alexiev, U. (2009) Surface charge changes upon formation of the signaling state in visual rhodopsin. *Photochem. Photobiol. 85*, 501–508.
8. Scherrer, P., Alexiev, U., Heyn, M. P., Marti, T., and Khorana, H. G. (1992) Structures and Functions of Retinal Proteins, Vol. *221*, Colloque INSERM/John Libbey Eurotext Ltd.
9. Wald, G., and Brown, P. K. (1953) The molar extinction of rhodopsin. *J. Gen. Physiol. 37*, 189–200.
10. Grassetti, D. R., and Murray, J. F., Jr. (1967) Determination of sulfhydryl groups with 2,2′- or 4,4′-dithiodipyridine. *Arch. Biochem. Biophys. 119*, 41–49.
11. Kim, T. Y., Winkler, K., and Alexiev, U. (2007) Picosecond multidimensional fluorescence spectroscopy: a tool to measure real-time protein dynamics during function. *Photochem. Photobiol. 83*, 378–384.
12. Farrens, D. L., and Khorana, H. G. (1995) Structure and function in rhodopsin. Measurement of the rate of metarhodopsin II decay by fluorescence spectroscopy. *J. Biol. Chem. 270*, 5073–5076.
13. Wald, G., and Brown, P. K. (1950) The synthesis of rhodopsin from retinene(1). *Proc. Natl. Acad. Sci. U.S.A. 36*, 84–92.
14. Chen, Y. S., and Hubbell, W. L. (1978) Reactions of the sulfhydryl groups of membrane-bound bovine rhodopsin. *Membr. Biochem. 1*, 107–130.
15. Bucci, S., and Fagotti, C. (1991) Small-angle neutron-scattering study of ionic-nonionic mixed micelles. *Langmuir 7*, 824–826.
16. Turro, N. J., and Yekta, A. (1978) Luminescent probes for detergent solutions. A simple procedure for determination of the mean aggregation number of micelles. *J. Am. Chem. Soc. 100*, 5951–5952.
17. Tummino, P. J., and Gafni, A. (1993) Determination of the aggregation number of detergent micelles using steady-state fluorescence quenching. *Biophys. J. 64*, 1580–1587.
18. Alexiev, U., Rimke, I., and Pohlmann, T. (2003) Elucidation of the nature of the conformational changes of the EF-interhelical loop in bacteriorhodopsin and of the helix VIII on the cytoplasmic surface of bovine rhodopsin: a time-resolved fluorescence depolarization study. *J. Mol. Biol. 328*, 705–719.
19. Kirchberg, K., Kim, T. Y., Haase, S., and Alexiev, U. (2010) Functional interaction structures of the photochromic retinal protein rhodopsin. *Photochem. Photobiol. Sci. 9*, 226–233.
20. Krishna, A. G., Menon, S. T., Terry, T. J., and Sakmar, T. P. (2002) Evidence that helix 8 of rhodopsin acts as a membrane-dependent conformational switch. *Biochemistry 41*, 8298–8309.
21. Lehmann, N., Alexiev, U., and Fahmy, K. (2007) Linkage between the intramembrane H-bond network around aspartic acid 83 and the cytosolic environment of helix 8 in photoactivated rhodopsin. *J. Mol. Biol. 366*, 1129–1141.
22. Schroder, G. F., Alexiev, U., and Grubmuller, H. (2005) Simulation of fluorescence anisotropy experiments: probing protein dynamics. *Biophys. J. 89*, 3757–3770.
23. Kim, T. Y., Moeller, M., Winkler, K., Kirchberg, K., and Alexiev, U. (2009) Dissection of environmental changes at the cytoplasmic surface of light-activated bacteriorhodopsin and visual rhodopsin: sequence of spectrally silent steps. *Photochem. Photobiol. 85*, 570–577.
24. Dornmair, K., Kiefer, H., and Jahnig, F. (1990) Refolding of an integral membrane protein. OmpA of *Escherichia coli*. *J. Biol. Chem. 265*, 18907–18911.
25. Lau, F. W., and Bowie, J. U. (1997) A method for assessing the stability of a membrane protein. *Biochemistry 36*, 5884–5892.
26. London, E., and Khorana, H. G. (1982) Denaturation and renaturation of bacteriorhodopsin in detergents and lipid-detergent mixtures. *J. Biol. Chem. 257*, 7003–7011.
27. Otzen, D. E. (2003) Folding of DsbB in mixed micelles: a kinetic analysis of the stability of a bacterial membrane protein. *J. Mol. Biol. 330*, 641–649.
28. Tanford, C. (1991) The Hydrophobic Effect. Formation of Micelles and Biological Membranes, 2nd ed., Wiley and Sons, New York.
29. Mascher, E., and Lundahl, P. (1989) Sodium dodecyl sulphate-protein complexes: Changes in size or shape below the critical micelle concentration, as monitored by high-performance agarose gel chromatography. *J. Chromatogr. 476*, 147–158.
30. Ibel, K., May, R. P., Kirschner, K., Szadkowski, H., Mascher, E., and Lundahl, P. (1990) Protein-decorated micelle structure of sodium-dodecyl-sulfate−protein complexes as determined by neutron scattering. *Eur. J. Biochem. 190*, 311–318.
31. Jirgensons, B. (1967) Effects of n-propyl alcohol and detergents on the optical rotatory dispersion of alpha-chymotrypsinogen, beta-casein, histone fraction F1, and soybean trypsin inhibitor. *J. Biol. Chem. 242*, 912–918.
32. Mattice, W. L., Riser, J. M., and Clark, D. S. (1976) Conformational properties of the complexes formed by proteins and sodium dodecyl sulfate. *Biochemistry 15*, 4264–4272.
33. Rao, J. K., and Argos, P. (1981) Structural stability of halophilic proteins. *Biochemistry 20*, 6536–6543.
34. Otzen, D. E. (2002) Protein unfolding in detergents: effect of micelle structure, ionic strength, pH, and temperature. *Biophys. J. 83*, 2219–2230.
35. Otzen, D. E., and Oliveberg, M. (2002) Burst-phase expansion of native protein prior to global unfolding in SDS. *J. Mol. Biol. 315*, 1231–1240.
36. Alexiev, U., Mollaaghababa, R., Khorana, H. G., and Heyn, M. P. (2000) Evidence for long range allosteric interactions between the extracellular and cytoplasmic parts of bacteriorhodopsin from the mutant R82A and its second site revertant R82A/G231C. *J. Biol. Chem. 275*, 13431–13440.
37. Heyne, K., Herbst, J., Dominguez-Herradon, B., Alexiev, U., and Diller, R. (2000) Reaction control in bacteriorhodopsin: impact of Arg82 and Asp85 on the fast retinal isomerization, studied in the second site revertant Arg82Ala/Gly231Cys and various purple and blue forms of bacteriorhodopsin. *J. Phys. Chem. B 104*, 6053–6058.
38. Alexiev, U., Scherrer, P., Marti, T., Khorana, H. G., and Heyn, M. P. (1995) Time-resolved surface charge change on the cytoplasmic side of bacteriorhodopsin. *FEBS Lett. 373*, 81–84.
39. Cai, K., Klein-Seetharaman, J., Farrens, D., Zhang, C., Altenbach, C., Hubbell, W. L., and Khorana, H. G. (1999) Single-cysteine substitution mutants at amino acid positions 306−321 in rhodopsin, the sequence between the cytoplasmic end of helix VII and the palmitoylation sites: sulfhydryl reactivity and transducin activation reveal a tertiary structure. *Biochemistry 38*, 7925–7930.
40. Klein-Seetharaman, J., Hwa, J., Cai, K., Altenbach, C., Hubbell, W. L., and Khorana, H. G. (1999) Single-cysteine substitution mutants at amino acid positions 55−75, the sequence connecting the cytoplasmic ends of helices I and II in rhodopsin: reactivity of the sulfhydryl groups and their derivatives identifies a tertiary structure that changes upon light-activation. *Biochemistry 38*, 7938–7944.
41. Croonen, Y., Gelade, E., Van der Zegel, M., Van der Auweraer, M., Vandendriessche, H., De Schryver, F. C., and Almgren, M. (1983) Influence of salt, detergent concentration, and temperature on the fluorescence quenching of 1-methylpyrene in sodium dodecyl sulfate with m-dicyanobenzene. *J. Phys. Chem. 87*, 1426–1431.
42. Sreerama, N. a. W., R.W. (2000) Estimation of protein secondary structure from circular dichroism spectra: comparison of CONTIN, SELCON, and CDSSTR methods with an expanded reference set. *Anal. Biochem. 287*, 252–260.